GSA Data Repository 2017242

Evolution of shear fabric in granular fault gouge from stable sliding to stick slip and implications for fault slip mode

M.M. Scuderi[1], C. Collettini[1], C. Viti[2], E. Tinti[3] and C. Marone[4]

[1]*Department of Earth Sciences, University of Rome La Sapienza, 00185 Rome, Italy*
[2]*Department of Physical Sciences, Earth and Environment, University of Siena, 53100 Siena, Italy*
[3]*National Institute of Geophysics and Volcanology (INGV), 00143Rome, Italy*
[4]*Department of Geoscience, The Pennsylvania State University, University Park, Pennsylvania 16801, USA*

*Correspondence to: marco.scuderi@uniroma1.it

This file includes text, figures and tables divided into seven Data Repository (DR) items:

- Table DR1 Summary of experiments and boundary conditions;
- Figure DR1 Evaluation of rate and state friction parameters;
- Figure DR2 Calculation of the dilatancy coefficient
- Figure DR3 Details on fabric evolution from stable sliding to stick-slip;
- Figure DR4 Characterization of the stiffness of the loading system;
- Figure DR5 Growing of frictional instabilities for a typical experiment;
- Figure DR6 The role of applied normal stress in the stiffness of the loading system.

Table DR1: Summary of experiments and boundary conditions.

Experiment number	Normal stress (MPa)	Spring	Target of the experiment	Microscopy analyses
b266	13	Yes	Stable Sliding	No
b267	14	Yes	Stick-slip	No
b268	13.5	Yes	Stable sliding	No
b371	15	Yes	Stick-slip	SEM
b372	25	Yes	Stick-slip	No
b390	15	Yes	Stick-slip	SEM
b391	25	Yes	Stick-slip	SEM/TEM
b416	15	No	Rate & State friction parameters	No
b417	25	Yes	Stick-slip	No
b417	25	Yes	Stick-slip	No
b418	20	Yes	Stick-slip	No
b418	20	Yes	Stick-slip	No
b433	25	No	Rate & State friction parameters	No
b511	25	No	Stable sliding $\gamma = 4$	SEM
b512	25	No	Stable sliding $\gamma = 15$	SEM
b540	30	Yes	Stick-slip	SEM
b540	30	Yes	Stick-slip	SEM
b541	35	Yes	Stick-slip	SEM
b542	15	Yes	Stick-slip	SEM
b543	35	Yes	Stick-slip	SEM
b544	35	Yes	Stick-slip	SEM/TEM
b615	35	Yes	Stiffness during loading/unloading	No
b616	15	Yes	Stiffness during loading/unloading	No
b617	35,15	Yes	Stiffness during loading/unloading	No

All tests were conducted under 100% relative humidity (RH) to ensure experimental reproducibility. All experiments were run at shear velocity of 10 μm/s, except for experiments to retrieve RSF parameter, which included velocity steps tests of 1-3-10 μm/s.

Figure DR 1: Evaluation of rate and state friction parameters

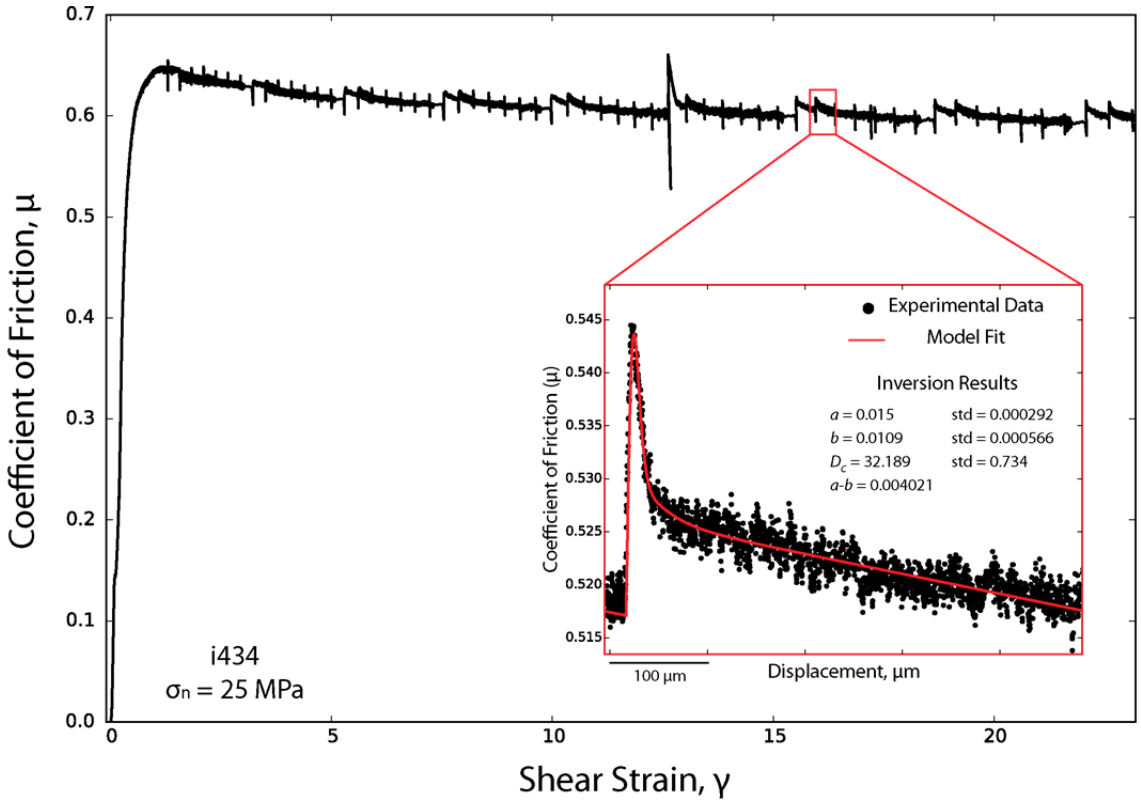

Figure DR1. To characterize the evolution of the rate- and state-friction parameters we performed a series of velocity steps (from 1 to 10 μm/s) with increasing strain, at normal stresses of 15 and 25 MPa. To determine the rate- and state-friction parameters, *(a-b)* and D_c, we modelled each velocity step using an iterative singular value decomposition technique, which solves the rate- and state-friction equations using the Ruina evolution law coupled with the elastic interaction of the testing machine (Reinen and Weeks, 1993; Blanpied et al., 1998). The inset in red shows the details of one velocity step with the comparison between experimental data (in black) and the result from the inversion model (red).

Figure DR2: Calculation of the dilatancy coefficient

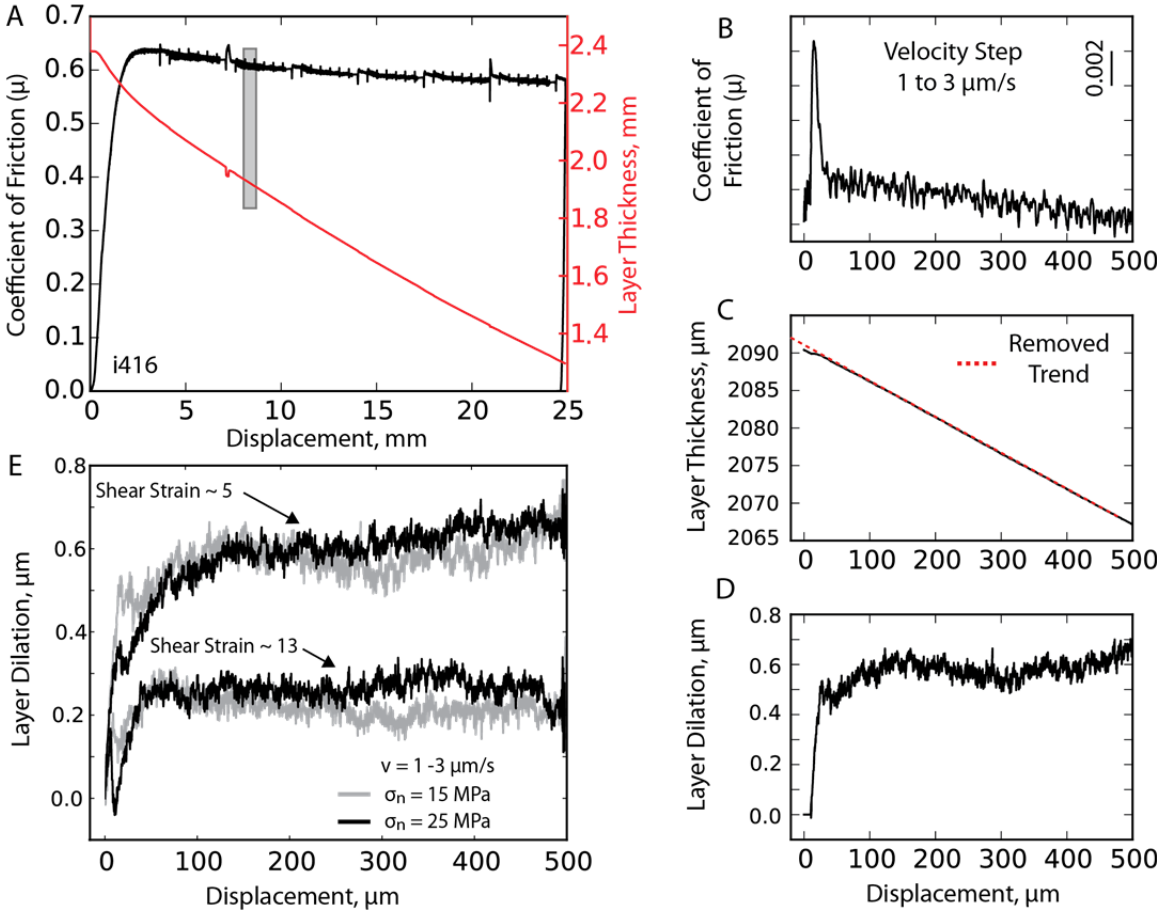

Figure DR2. In order to investigate the degree of shear localization in response to step changes in the imposed slip velocity, we analyzed changes in gouge layer thickness measured at constant normal stress. (Panel A) Data from a typical velocity step test. Note overall geometric layer thinning with superimposed variations. Dilation associated with velocity perturbations was measured after removing geometric layer thinning due to simple shear (Scott et al., 1994). (B) Enlargement of a velocity step (grey box in Panel A), showing the evolution of frictional strength; a linear trend has been removed. (C) Raw data for layer thickness evolution during the velocity step shown in (B). Dashed red line represents the linear trend removed in order to analyze dilation, as in panel D. (D) Detrended data from Panel C showing layer dilation at higher slip velocity. (E) Comparison of layer dilation at two values of shear strain for experiments performed at 15 (grey) and 25 MPa (black) normal stress. Data have been offset so that 0,0 corresponds to the velocity step. Note that for both normal stresses the instantaneous dilation is smaller at higher strain, indicating a greater degree of shear localization

Figure DR3: Details on fabric evolution from stable sliding to stick-slip

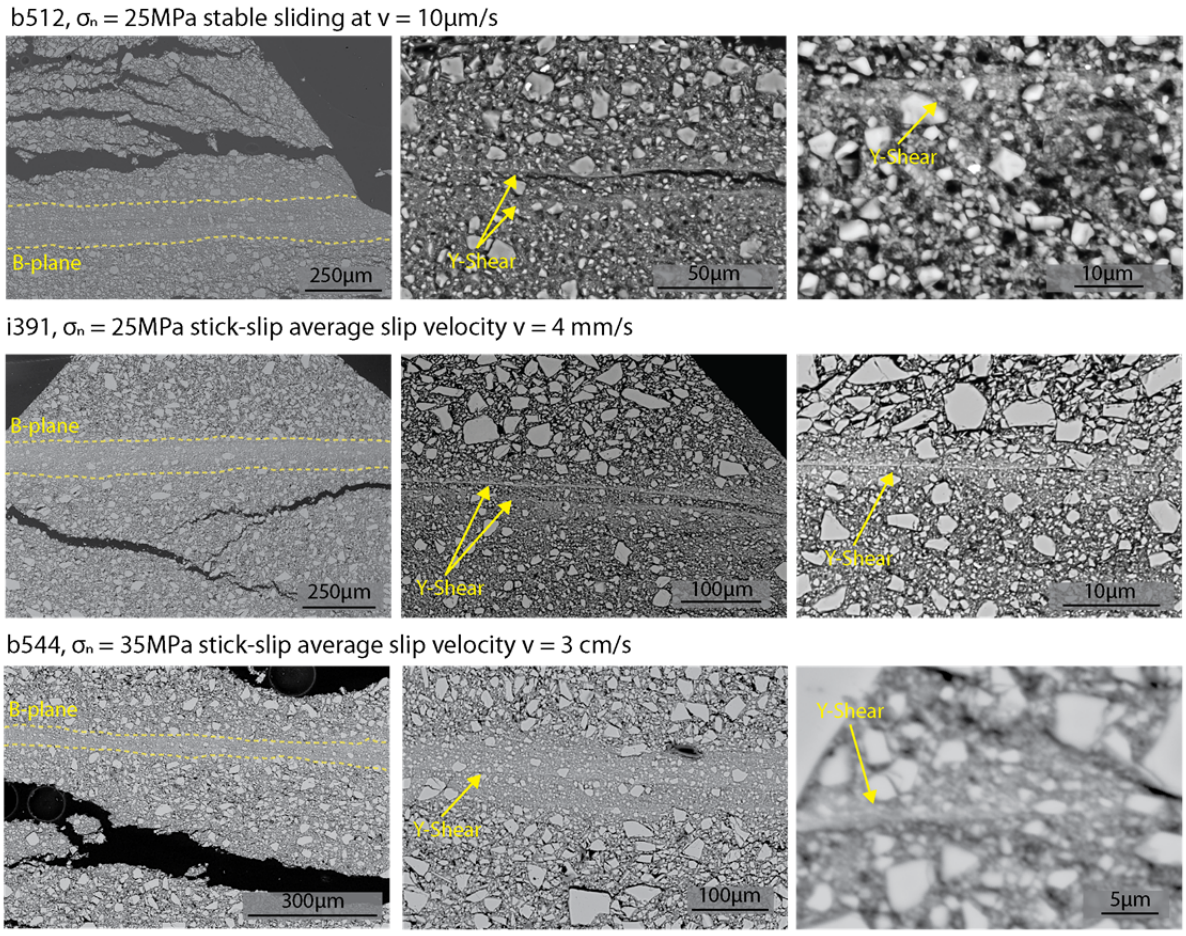

Microstructures for gouge layers sheared at different normal stresses and loading stiffnesses. Lower two rows are layers from dynamic, stick-slip failure. Upper row is a stable sliding experiment. Despite the different stick-slip velocities the microstructures are nearly identical. Note localization along Y-shear planes contained within B shear zones for each case. In these zones of localization the only difference between stable and unstable failure is that for higher stick-slip velocities the B shear zones show a higher level of grain-size reduction.

Figure DR3 continued

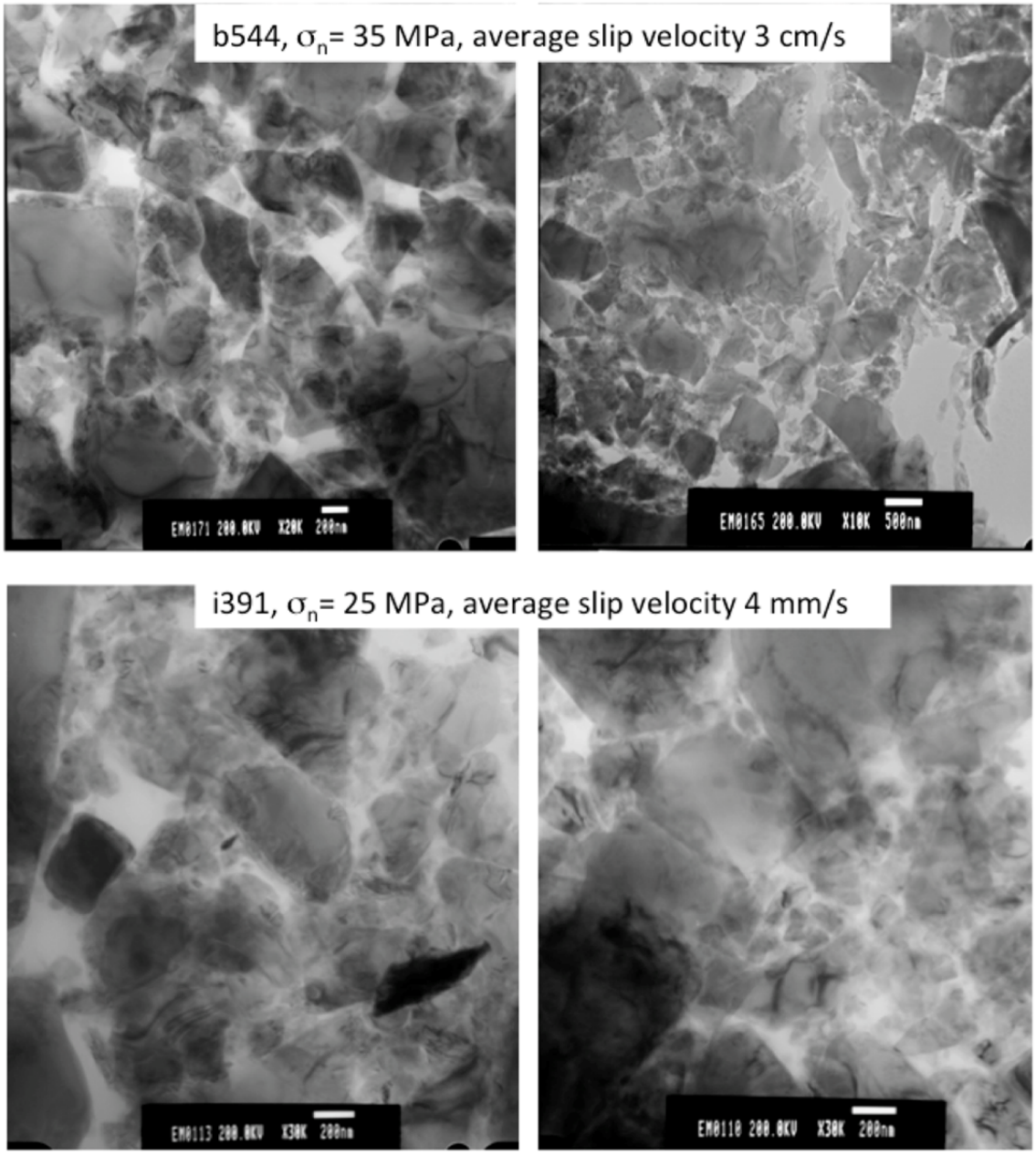

Details of the nanostructure of Y-shear planes for different stick-slip experiments. Nano-scale structures are very similar for the two boundary conditions; each consisting of nanograins, with grain-size of < 500 nm, with intense dislocations. Nanograins likely form by dislocation pile-up during strain accumulation.

Figure DR3 continued

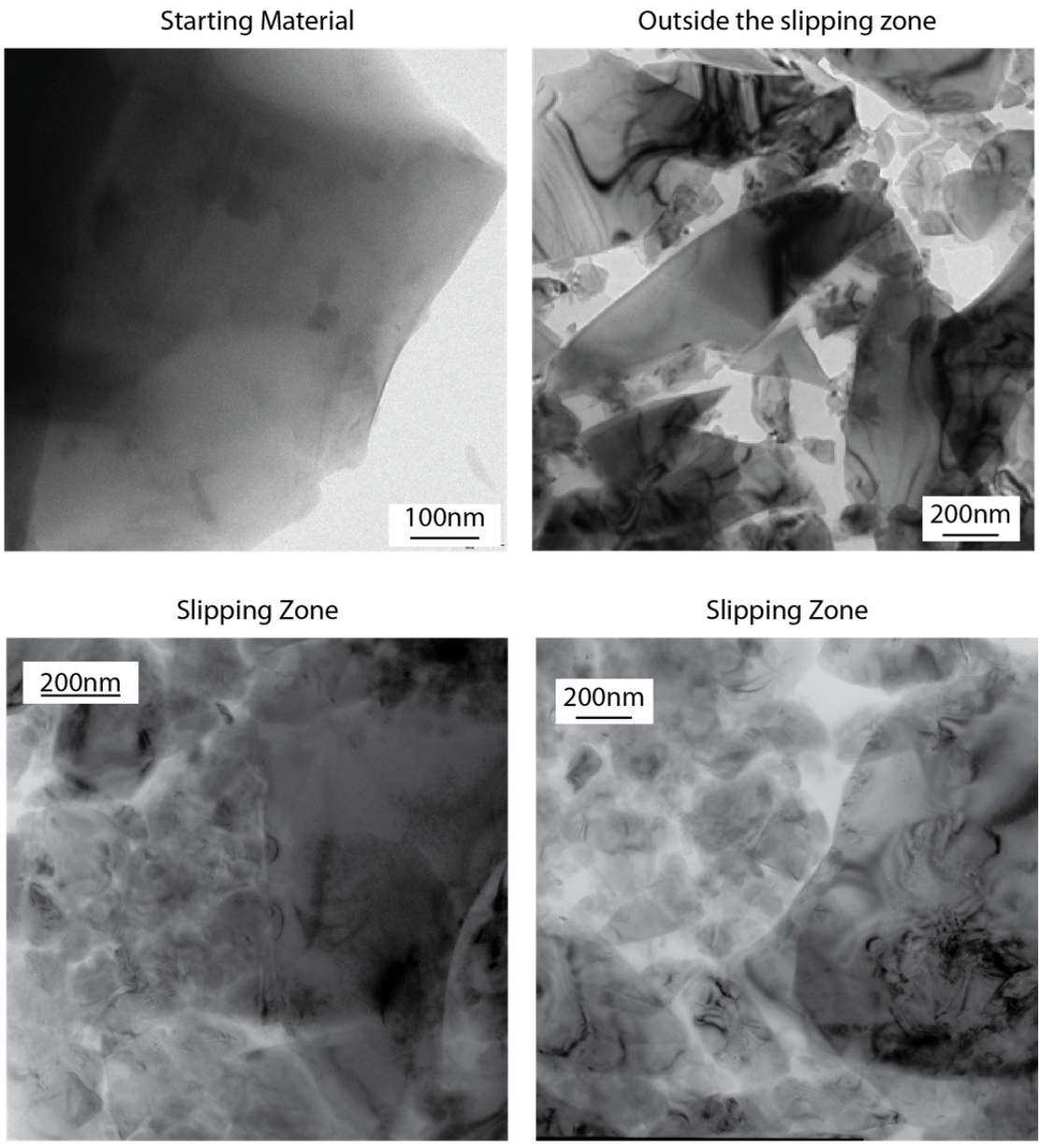

Bright-field phase-contrast images showing the occurrence of dislocations through the so-called dark contrast features. Grains from the starting material (top left) were invariably contrast-free, independently from crystal orientation (i.e., the grains were perfectly homogeneous also during crystal titlting under the TEM beam). Also, grains outside the slipping zone are angular with few dark contrast features indicating low degree of internal deformation. Conversely, grains in the shear zones are more rounded and always characterized by dark contrast features, indicating a high level of internal deformation (i.e. dislocations).

Figure DR3 continued

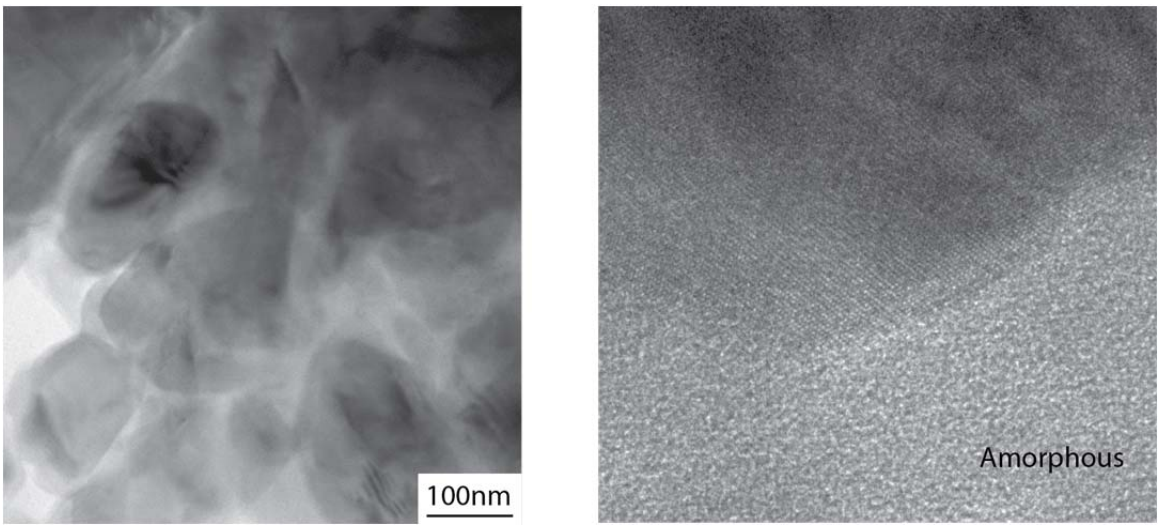

Thin amorphous films surrounding the surface of grains along the highly localized slipping zone.

Figure DR4: Characterization of the stiffness of the loading system.

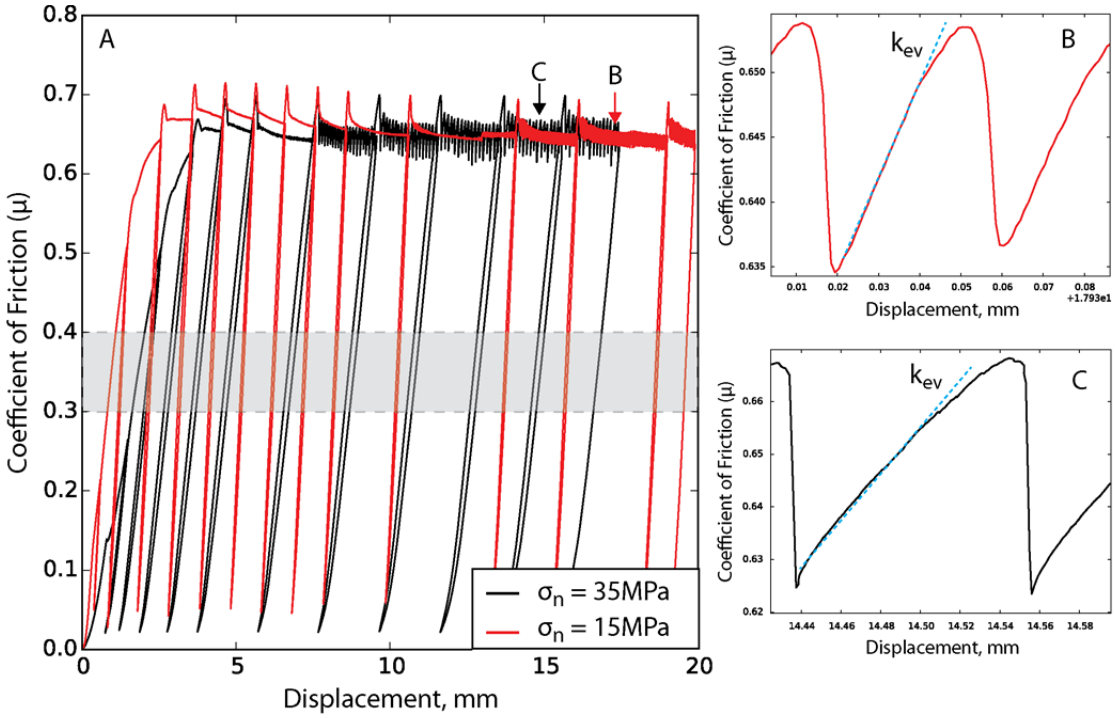

Figure DR4. Data showing the technique used to measure loading stiffness as a function of shear stress and shear strain. The effective loading stiffness is determined by apparatus stiffness, fault gouge stiffness, and normal stress: $k' = k/\sigma'_n$. We evaluate k from load/unload cycles (panel A) and from (panels B and C) the linear, elastic sections of the stick-slip loading curves. Both methods produce similar values, indicating that the shear stress dependence of k' is minor.

Figure DR5: Growth of frictional instabilities

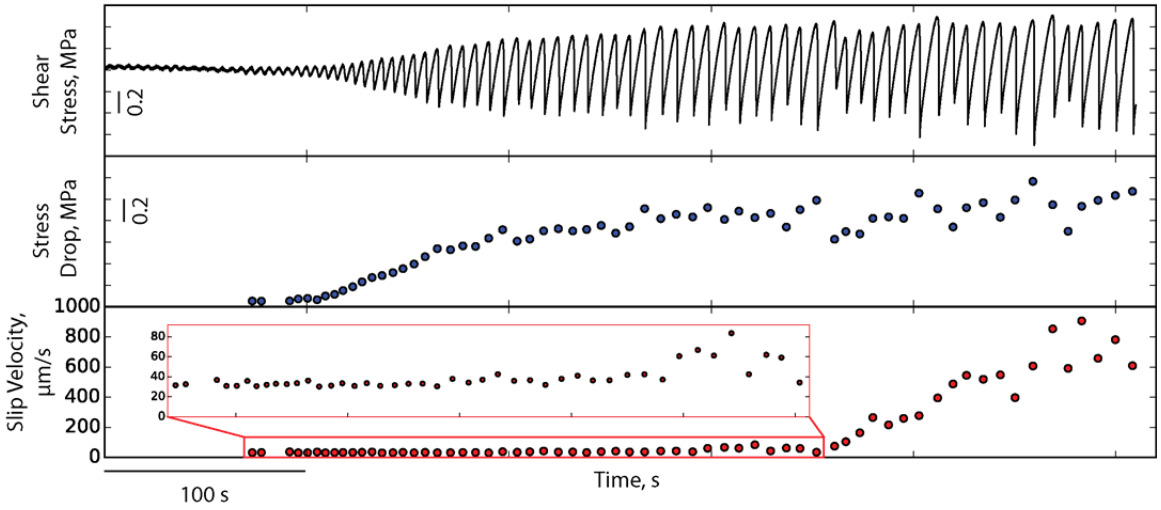

Figure DR5. Here we show an example of the spontaneous emergence of unstable sliding with small stick-slip instabilities that initiate when K = 1, i.e. near the intersection between black and red curves in figure 3. With increasing displacement we observe a growing phase in stress drop and slip velocity before reaching a nearly steady state, stick-slip behaviour.

Figure DR6: The role of applied normal stress in the stiffness of the loading system.

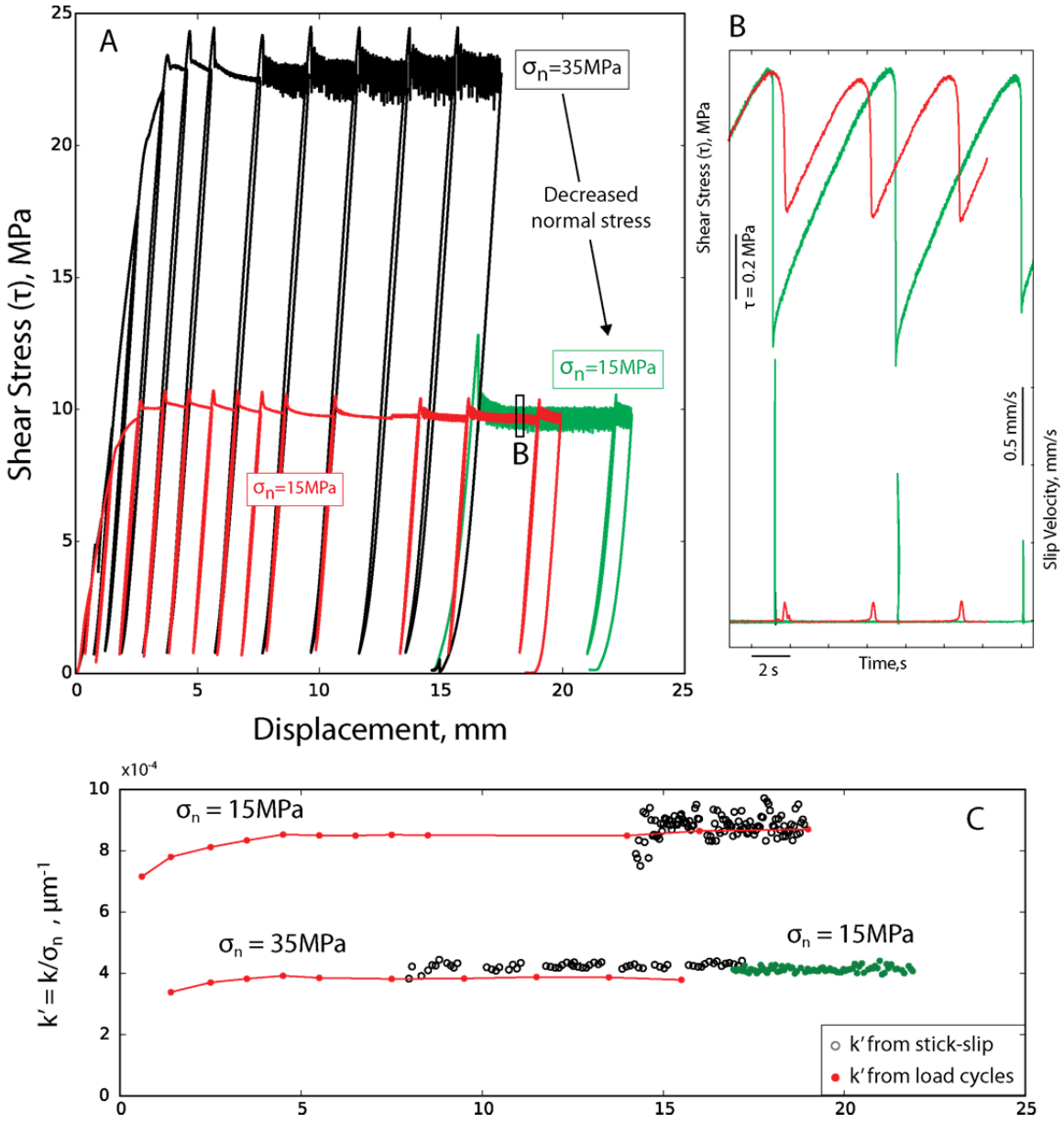

Figure DR6. Elastic stiffness *k* and its evolution with shear displacement and normal stress. (A) Data for *k* at two normal stresses as determined from load/unload cycles. Red line shows data for an experiment at 15 MPa normal stress. Black and green lines show an experiment that started at 35 MPa normal stress and was reduced to 15 MPa after ~ 15 mm of shear displacement. Note that sliding is unstable for the run in which normal stress was reduced. These stick-slips are different in comparison to the "standard" stick-slips observed at 15 MPa (red curves in figure B) because they have shorter duration of

the stress drop, larger stress drop (1.0 vs. 0.5 MPa), shorter rise time and faster slip velocity (1.5 vs. 0.15 mm/s). These faster stick-slip events recorded at 15 MPa result from a decrease of the stiffness of the loading system that it is acquired at 35 MPa and it is maintained when the normal stress is reduced at 15 MPa (Figure C). We interpret this increase in stiffness as a product of fabric development and fault zone stiffness. In particular the lower stiffness of the loading system is likely promoted by a more pronounced grain-size reduction favoured by higher stresses rather than stick-slip velocities, because stable values of stiffness at 35 MPa are reached after 5 mm of displacement, hence before the onset of stick-slip instabilities

References:

Blanpied, M.L.; Marone, C.J.; Lockner, D.A.; Byerlee, J.D.; King, D. P. . Quantitative measure of the variation in fault rheology due to fluid-rock interaction. *J. Geophys. Res.* **103,** 9691–9712 (1998).

Reinen, L. & Weeks, J. Determination of Rock Friction Constitutive Parameters Using an Iterative Least Squares Inversion Method. *J. Geophys. Res.* **98,** (1993).

Samuelson, J., D. Elsworth, and C. Marone (2009), Shear-induced dilatancy of fluid-saturated faults: Experiment and theory, *J. Geophys. Res.*, *114*(B12), B12404, doi:10.1029/2008JB006273.

Scott, D., C. Marone, and C. G. Sammis (1994), The apparent friction of granular fault gouge in sheared layers, *J. Geophys. Res.*, *99*, 7231–7246.